

Out-of-equilibrium phase re-entrance(s) in long-range interacting systemsF. Staniscia,^{1,2} P. H. Chavanis,^{3,4} G. De Ninno,^{2,5} and D. Fanelli⁶¹*Dipartimento di Fisica, Università di Trieste, 34127 Trieste, Italy*²*Sincrotrone Trieste, S.S. 14 km 163.5, Basovizza, 34149 Trieste, Italy*³*Laboratoire de Physique Théorique (IRSAMC), Université de Toulouse, UPS, F-31062 Toulouse, France*⁴*Laboratoire de Physique Théorique (IRSAMC), CNRS, F-31062 Toulouse, France*⁵*Physics Department, Nova Gorica University, 5001 Nova Gorica, Slovenia*⁶*Dipartimento di Energetica “Sergio Stecco,” Università di Firenze, via S. Marta 3, 50139 Firenze, Italy*

(Received 13 March 2009; revised manuscript received 9 July 2009; published 31 August 2009)

Systems with long-range interactions display a short-time relaxation toward quasistationary states (QSSs) whose lifetime increases with system size. The application of Lynden-Bell’s theory of “violent relaxation” to the Hamiltonian Mean Field model leads to the prediction of out-of-equilibrium first- and second-order phase transitions between homogeneous (zero magnetization) and inhomogeneous (nonzero magnetization) QSSs, as well as an interesting phenomenon of phase re-entrances. We compare these theoretical predictions with direct N -body numerical simulations. We confirm the existence of phase re-entrance in the typical parameter range predicted from Lynden-Bell’s theory, but also show that the picture is more complicated than initially thought. In particular, we exhibit the existence of secondary re-entrant phases: we find unmagnetized states in the theoretically magnetized region as well as persisting magnetized states in the theoretically unmagnetized region. We also report the existence of a region with negative specific heats for QSSs both in the numerical and analytical caloric curves.

DOI: [10.1103/PhysRevE.80.021138](https://doi.org/10.1103/PhysRevE.80.021138)

PACS number(s): 05.20.-y, 05.70.Fh, 05.45.-a, 52.65.Ff

I. INTRODUCTION

In statistical physics, phase re-entrance is a quite typical phenomenon occurring in many physical systems, such as spin-glasses, colloids, and polymers, in which there is a competition between different entropic terms [1–6]. A phase re-entrance is normally associated with inverse melting, a counterintuitive phenomenon in which isobaric addition of heat causes a disordered (e.g., liquid) phase to crystallize, the reverse of the usual situation. Phase re-entrance occurs when, providing additional heating to the system, the latter undergoes a new transition, from the ordered to the disordered phase. The phenomenon of phase re-entrance has been widely studied at thermodynamic equilibrium in systems whose constituents interact through short-range forces.

In this paper we give evidence to the existence of phase re-entrance also in the case of long-range interacting systems in out-of-equilibrium dynamical conditions.

Long-range interactions are such that the two-body interaction potential decays at large distances with a power-law exponent which is smaller than the space dimension. The dynamical and thermodynamical properties of these systems were poorly understood until a few years ago, and their study was essentially restricted to astrophysics (stellar systems) and two-dimensional turbulence (large-scale vortices) [7]. Later, it was recognized that long-range systems exhibit universal, albeit unconventional, equilibrium and out-of-equilibrium features [8]. It is for instance well-known that such systems get trapped in long-lasting quasistationary states (QSS) [9–16], before relaxing to thermal equilibrium. The duration of a QSS increases with the number of particles N in the system. Remarkably, when the thermodynamic limit ($N \rightarrow \infty$) is performed before the infinite time limit ($t \rightarrow +\infty$), the system remains permanently trapped in QSSs. As a con-

sequence, QSSs represent the only accessible experimental dynamical regimes for systems composed by a large number of long-range interacting particles. This includes systems of paramount importance, such as non-neutral plasmas confined by a strong magnetic field [17,18], free-electron lasers [19], and ion particle beams [20]. The ubiquity of QSSs has originated an intense debate [21] about the mechanisms responsible for their emergence, their persistence, and their eventual evolution toward statistical equilibrium. In fact, QSSs keep memory of the initial condition and, as a consequence, they cannot be interpreted by making use of the classical Boltzmann-Gibbs approach.

In a series of recent papers [22–26], an approximate analytical theory based on the Vlasov equation and inspired by a seminal work of Lynden-Bell [27] in astrophysics has been proposed. This is a fully predictive approach, enabling one to explain the emergence and the properties of QSSs from first principles [28].

In this paper we utilize a well-known Hamiltonian toy model, the so-called Hamiltonian mean field (HMF) model [29], to demonstrate that phase re-entrance(s) may also occur in a long-range interacting system, dynamically trapped in a QSS. The HMF describes the motion of N rotators, coupled through an equal strength cosine interaction. The Hamiltonian reads

$$H = \frac{1}{2} \sum_{j=1}^N p_j^2 + \frac{1}{2N} \sum_{i,j=1}^N [1 - \cos(\theta_j - \theta_i)], \quad (1)$$

where θ_j represents the orientation of the j -th rotator and p_j stands for its conjugated momentum. To monitor the evolution of the systems it is customary to introduce the magnetization, an order parameter defined as

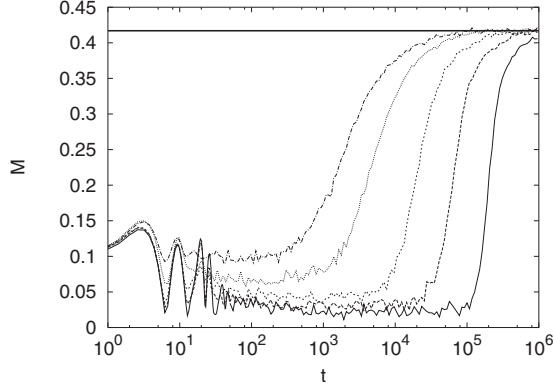


FIG. 1. Magnetization as a function of time, for systems with different sizes. The continuous, dashed, short-dashed, dotted, and dot-dashed lines correspond, respectively, to $N=2 \cdot 10^4$, 10^4 , $5 \cdot 10^3$, $2 \cdot 10^3$, 10^3 . We see that QSSs start approximately at $t=40$, and their duration increases with the system size; eventually, they relax to Boltzmann equilibrium (thick line). Simulations are performed starting from a two-level distribution with energy $U=0.6400$, $f_0=0.094$, and averaging over different system realizations with the same initial distribution (50, 100, 200, 500, and 1000, respectively).

$$M = \frac{|\sum_i \mathbf{m}_i|}{N} \quad \text{where} \quad \mathbf{m}_i = (\cos \theta_i, \sin \theta_i). \quad (2)$$

The infinite-range coupling between rotators, provides the system with all typical characteristics of a long-range system, as clearly displayed in Fig. 1. Here, the magnetization is monitored as a function of time: after an initial “violent” relaxation, the system reaches a QSS, which is followed by a slow relaxation toward Boltzmann statistical equilibrium. The larger the system, the longer the intermediate phase where it remains confined before reaching the final equilibrium.

The paper is organized as follows: in Sec. II, we present the continuous Vlasov picture and review the maximum entropy principle based on the Lynden-Bell approach. This theoretical setting is used to obtain the HMF phase diagrams in different representations from which out-of-equilibrium phase transitions [22–26] and phase re-entrance [22,26] can be predicted. In Sec. III, these theoretical predictions are compared to N -body simulations based on (1). Finally, in Sec. IV we sum up our results and draw our conclusions.

II. OUT-OF-EQUILIBRIUM PHASE RE-ENTRANCE: THE PREDICTION OF LYNDEN-BELL THEORY

A. General theory and two-level approximation

In a recent series of papers [22–26], an approximate analytical theory based on the Vlasov equation has been proposed for the HMF model stemming from the seminal work of Lynden-Bell [27]. This is a fully predictive approach, justified from first principles, which captures most of the peculiar traits of the HMF out-of-equilibrium dynamics. The philosophy of the proposed approach is briefly reviewed in the following:

In the limit of $N \rightarrow \infty$, the HMF dynamics can be formally described using the Vlasov equation

$$\frac{\partial f}{\partial t} + p \frac{\partial f}{\partial \theta} - (M_x[f] \sin \theta - M_y[f] \cos \theta) \frac{\partial f}{\partial p} = 0, \quad (3)$$

where $f(\theta, p, t)$ is the one-body microscopic distribution function (DF), and the two components of the magnetization are, respectively, given by

$$M_x[f] = \int f \cos \theta d\theta dp,$$

$$M_y[f] = \int f \sin \theta d\theta dp. \quad (4)$$

The mean-field energy can be expressed as

$$U = \frac{1}{2} \int f p^2 d\theta dp - \frac{M_x^2 + M_y^2}{2} + \frac{1}{2}. \quad (5)$$

Working in this setting, it can be then hypothesized that QSSs correspond to stable stationary equilibria of the Vlasov equation on a coarse-grained scale. Lynden-Bell’s idea goes as follows: the Vlasov dynamics induces a progressive filamentation of the initial single-particle distribution profile, i.e., the continuous counterpart of the discrete N -body distribution, which proceeds at smaller and smaller scales without reaching an equilibrium. Conversely, at a coarse-grained level, the process comes to an end, and the distribution-function $\bar{f}_{QSS}(\theta, p, t)$, averaged over a finite grid, eventually converges to an asymptotic form. Following Lynden-Bell, one can then associate a mixing entropy to this process. Assuming ergodicity (i.e., efficient mixing), $\bar{f}_{QSS}(\theta, p)$, is obtained by maximizing the mixing entropy, while imposing the conservation of Vlasov dynamical invariants. It is worth emphasizing that the prediction of the QSS depends on the details of the initial condition [30], not only on the values of energy and mass as for the Boltzmann statistical equilibrium state.

For a two-level initial condition $f(\theta, p, t=0) \in \{0, f_0\}$, the Lynden-Bell entropy is explicitly constructed from the coarse-grained distribution function \bar{f} as [22,31]

$$S[\bar{f}] = - \int dp d\theta \left[\frac{\bar{f}}{f_0} \ln \frac{\bar{f}}{f_0} + \left(1 - \frac{\bar{f}}{f_0}\right) \ln \left(1 - \frac{\bar{f}}{f_0}\right) \right]. \quad (6)$$

We thus have to solve the maximization problem

$$\max_{\bar{f}} \left\{ S[\bar{f}] \mid U[\bar{f}] = U, \quad \mathcal{M}[\bar{f}] \equiv \int \bar{f} d\theta dp = 1 \right\}. \quad (7)$$

This maximization problem assures that the distribution function is thermodynamically stable (most probable macrostate) in the sense of Lynden-Bell [27] and also that it is nonlinearly dynamically stable with respect to the Vlasov equation [32]. From Eq. (6), we write the first-order variations as $\delta S - \beta \delta U - \alpha \delta \mathcal{M} = 0$, where the inverse temperature $\beta = 1/T$ and the “chemical-potential” α are Lagrange multipliers associated with the conservation of energy and mass.

Requiring that this functional is stationary, one obtains the following distribution [22–24]:

$$\bar{f}_{QSS}(\theta, p) = \frac{f_0}{1 + e^{\beta(p^2/2 - M_x[\bar{f}_{QSS}] \cos \theta - M_y[\bar{f}_{QSS}] \sin \theta) + \alpha}}. \quad (8)$$

As a general remark, it should be emphasized the “fermionic” form of the distribution, which arises because of the form of the entropy. Notice also that the magnetization is related self-consistently to the distribution function by Eq. (4), and the problem hence amounts to solving an *integro-differential* equation. In doing so, we have also to make sure that the critical point corresponds to an entropy maximum, not to a minimum or a saddle point. Let us now insert expression (8) into the energy and normalization constraints and use the definition of magnetization (4). Further, defining $\lambda = e^\alpha$ and $\mathbf{m} = (\cos \theta, \sin \theta)$ yields [38]

$$\begin{aligned} f_0 \sqrt{\frac{2}{\beta}} \int d\theta I_{-1/2}(\lambda e^{-\beta \mathbf{M} \cdot \mathbf{m}}) &= 1, \\ f_0 \frac{1}{2} \left(\frac{2}{\beta}\right)^{3/2} \int d\theta I_{1/2}(\lambda e^{-\beta \mathbf{M} \cdot \mathbf{m}}) &= U + \frac{M^2 - 1}{2}, \\ f_0 \sqrt{\frac{2}{\beta}} \int d\theta \cos \theta I_{-1/2}(\lambda e^{-\beta \mathbf{M} \cdot \mathbf{m}}) &= M_x, \\ f_0 \sqrt{\frac{2}{\beta}} \int d\theta \sin \theta I_{-1/2}(\lambda e^{-\beta \mathbf{M} \cdot \mathbf{m}}) &= M_y, \end{aligned} \quad (9)$$

where we have defined the Fermi integrals

$$I_n(t) = \int_0^{+\infty} \frac{x^n}{1 + t e^x} dx. \quad (10)$$

Their asymptotic limits are recalled in Ref. [22].

If we consider spatially homogeneous configurations ($M_{QSS} = 0$), the Lynden-Bell distribution becomes

$$\bar{f}_{QSS}(p) = \frac{f_0}{1 + \lambda e^{\beta p^2/2}}. \quad (11)$$

In the nondegenerate limit $\lambda \rightarrow +\infty$, the latter reduces to the Boltzmann distribution $\bar{f} = (\beta/2\pi)^{1/2} e^{-\beta p^2/2}$ and in the completely degenerate limit $\lambda \rightarrow 0$, it becomes a step function: $\bar{f} = f_0$ for $|p| < 1/(4\pi f_0)$ and $\bar{f} = 0$ otherwise. If we make use of Eq. (9), we get the caloric curve $\beta(U)$ for a fixed value of f_0 parametrized by λ [22]

$$U - \frac{1}{2} = \frac{1}{8\pi^2 f_0^2} \frac{I_{1/2}(\lambda)}{I_{-1/2}(\lambda)^3}, \quad (12)$$

$$\beta = 8\pi^2 f_0^2 I_{-1/2}(\lambda)^2. \quad (13)$$

The homogeneous Lynden-Bell distribution with fixed value of f_0 exists only for [22]

$$U \geq U_{\min}(f_0) \equiv \frac{1}{96\pi^2 f_0^2} + \frac{1}{2}. \quad (14)$$

Let us now address the problem of stability of the homogeneous Lynden-Bell distribution. In Ref. [22] it has been shown that the critical curve $U_c(f_0)$ separating stable and unstable homogeneous Lynden-Bell distributions is given by the parametric Eq. (12) and

$$I_{-1/2}(\lambda) \lambda |I'_{-1/2}(\lambda)| = \frac{1}{(2\pi f_0)^2}, \quad (15)$$

where λ goes from 0 to $+\infty$. In fact, the curve $U_c(f_0)$ delimitates the region where the homogeneous Lynden-Bell distribution is a *local* entropy maximum, at fixed mass and energy. If several local entropy maxima are found (for example, homogeneous and inhomogeneous Lynden-Bell distributions), we must compare their entropies to determine the stable state (global entropy maximum) and the metastable states (secondary entropy maxima). For systems with long-range interactions, metastable states have in general very long lifetimes, scaling like e^N , so that they are stable in practice and must absolutely be taken into account [33,34]. For this reason, (out-of-equilibrium) stability diagrams do not coincide with phase diagrams. In fact, the latter require a careful investigation of metastable states.

B. Phase diagram in the (f_0, U) plane

The phase diagram of the Lynden-Bell distribution in the (f_0, U) plane is shown in Fig. 2. We have also plotted the stability curve $U_c(f_0)$ of the homogeneous phase [split in two parts, $U_c^f(f_0)$ and $U_c^s(f_0)$] parameterized by λ . On the left of this curve, the homogeneous phase is stable (maximum entropy state) and on the right of this curve it is unstable (saddle point of entropy) [39]. For $f_0 \rightarrow +\infty$, the homogeneous Lynden-Bell distribution is stable only if $U \geq U_c = 3/4$ [22]. This is the critical energy associated with the Maxwell distribution (nondegenerate limit). On the line of minimum-energy $U = U_{\min}(f_0)$, we are in the completely degenerate limit $\lambda \rightarrow 0$ and the homogeneous Lynden-Bell distribution is stable when $f_0 \leq (f_0)_c = 1/(2\pi\sqrt{2})$, i.e., $U \geq U_c = 7/12$. This is the critical energy associated with the spatially homogeneous water-bag distribution. Therefore, the minimum-energy curve $U_{\min}(f_0)$ crosses the stability curve $U_c(f_0)$ at $((f_0)_c, U_c) \approx (0.1125, 0.5833)$.

If we now take into account Lynden-Bell’s inhomogeneous states, solving numerically Eq. (9), we find that the phase diagram displays first- and second-order phase transitions. The curve $U_c(f_0)$ splits in two curves $U_c^f(f_0)$ and $U_c^s(f_0)$. In the case of a second-order phase transition, the stability threshold corresponds to the transition between a homogeneous and an inhomogeneous distribution. The second-order phase transition corresponds to the branch $U_c^s(f_0)$. On the other hand, for a first-order phase transition, as we have the coexistence of two entropy maxima, the stability condition of the homogenous phase is no more sufficient to find the transition line, which has to be calculated by making a comparison between the two entropy maxima. This procedure has been followed to plot the line $U_r(f_0)$ in Fig. 2. This line of first-order phase transition is reached when the homogeneous and inhomogeneous phases have the same entropy. The line $U_r(f_0)$ (first order) and the line $U_c^s(f_0)$ (second

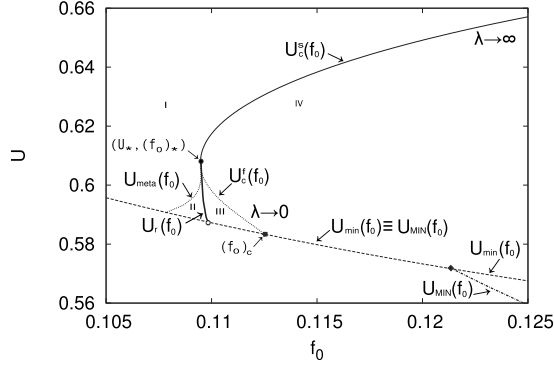


FIG. 2. Phase diagram in the (f_0, U) plane. The homogeneous phase only exists above the line $U_{\min}(f_0)$. The stability curve $U_c(f_0)$ is parameterized by λ . For $\lambda \rightarrow 0$ (completely degenerate limit), we get $f_0 = (f_0)_c = 1/(2\pi\sqrt{2})$ and $U_c = 7/12$. For $\lambda \rightarrow +\infty$ (nondegenerate limit), we get $f_0 \rightarrow +\infty$ and $U_c = 3/4$. On the left of this curve, the homogeneous phase is stable and on the right of this curve it is unstable. The stability curve is divided in two parts, i.e., $U_c^f(f_0)$ and $U_c^s(f_0)$, by the tricritical point (full round dot) located at $((f_0)_*, U_*)$. The continuous line corresponds to the second-order transition line. The thick line represents the first-order transition line while the dotted lines correspond to the borders of the metastable region. All these lines divide the diagram in four regions. In region (I), the homogeneous phase is stable and the inhomogeneous phase does not exist; in (II), the homogeneous phase is stable and the inhomogeneous phase metastable; in (III), the homogeneous phase is metastable and the inhomogeneous phase stable; in (IV) the homogeneous phase is unstable and the inhomogeneous phase stable. $U_{\min}(f_0)$ is the line below which the homogeneous phase does not exist, and $U_{\text{MIN}}(f_0)$ is the lowest accessible value of energy for a rectangular water-bag initial condition (see Sec. II E). The square dot is $[(f_0)_c, U_c((f_0)_c)]$, the diamond is $((f_0)_m, U_m)$ (Sec. II E), and the empty round dot is $[(f_0)_r, U_r((f_0)_r)]$. For $f_0 \in [(f_0)_*, (f_0)_c]$ there is a re-entrant phase.

order) merge together at a tricritical point, located at $((f_0)_*, U_*) \approx (0.10947, 0.608)$ and corresponding to $\lambda_* = 0.024$. We have also plotted the curves $U_c^f(f_0)$ and $U_{\text{meta}}(f_0)$ giving the lateral edges of the metastability regions for the homogeneous and inhomogeneous phases (see figure caption for more details).

In conclusion, the second-order phase transition occurs for a range of values of $U(f_0)$ bounded by the tricritical point $(U_*, (f_0)_*)$, and by $U_c = 3/4$, reached for $f_0 \rightarrow +\infty$. For $U > U_c = 3/4$, the Lynden-Bell theory always predicts a homogeneous phase (for any value of f_0). For $f_0 < (f_0)_*$, the homogeneous phase is always stable [for any $U \geq U_{\min}(f_0)$]. For $f_0 > (f_0)_c$, the homogeneous phase is stable for $U > U_c(f_0)$ and unstable for $U_{\min}(f_0) \leq U < U_c(f_0)$. The first-order phase transition occurs for a range of $U_c(f_0)$ bounded by the tricritical point $(U_*, (f_0)_*)$ and by the point $((f_0)_r, U_r((f_0)_r)) \approx (0.1098, 0.5875)$. As can be seen in Fig. 2, the theory predicts a phase re-entrance, for a set of values of $f_0 \in [(f_0)_*, (f_0)_c]$. This means that, decreasing U in the diagram at fixed $f_0 \in [(f_0)_*, (f_0)_c]$, the homogeneous phase is stable for $U > U_c^s(f_0)$, unstable for $U_c^f(f_0) < U < U_c^s(f_0)$, and stable again (or metastable) for $U_{\min}(f_0) < U < U_c^f(f_0)$. In the metastability region $U_{\min}(f_0) < U < U_c^f(f_0)$, the system can be found either in the homogeneous or inhomogeneous phase

depending on how it has been prepared initially (recall that metastable states are highly robust for systems with long-range interactions). By contrast, for $U_c^f(f_0) < U < U_c^s(f_0)$, the theory predicts an inhomogeneous phase and for $U > U_c^s(f_0)$ a homogeneous phase.

C. Phase diagram in the (M_0, U) plane

The preceding results are valid for *any* initial condition with two phase levels $f=0$ and $f=f_0$, whatever the number of patches and their shape. In the two-level case, the relevant control parameters are (f_0, U) [22]. They fully specify the Lynden-Bell equilibrium state from the initial condition. This means that, assuming ergodicity, the system remembers the initial condition through the values of these parameters. In this sense, the general phase diagram in the two-level case is the one represented in Fig. 2.

Now, many numerical simulations of the N -body system [23,25], or of the Vlasov equation [24], have been performed starting from a family of rectangular water-bag distributions. The latter correspond to assuming a constant value f_0 inside the phase-space domain D

$$D = \{(\theta, p) \in [-\pi, \pi] \times [-\infty, +\infty] \mid |\theta| < \Delta\theta, |p| < \Delta p\} \quad (16)$$

and zero outside. Here $0 \leq \Delta\theta \leq \pi$ and $\Delta p \geq 0$. The normalization condition results in

$$f_0 = \frac{1}{4\Delta\theta\Delta p}. \quad (17)$$

Notice that, for this specific choice, the initial magnetization M_0 and the energy density U can be expressed as functions of $\Delta\theta$ and Δp as

$$U = \frac{(\Delta p)^2}{6} + \frac{1 - (M_0)^2}{2}, \quad (18)$$

$$M_0 = \frac{\sin(\Delta\theta)}{\Delta\theta}. \quad (19)$$

For the case under scrutiny, $0 \leq M_0 \leq 1$ and $U \geq U_{\text{MIN}}(M_0) \equiv (1 - M_0^2)/2$. The energy $U_{\text{MIN}}(M_0)$ represents the absolute minimum accessible energy for a rectangular water-bag distribution with magnetization M_0 . The initial configuration is completely specified by the variables $(\Delta\theta, \Delta p)$ or, equivalently, by the variables (M_0, U) . On the other hand, for the determination of the Lynden-Bell equilibrium state, only the variables (f_0, U) matter. Now, we note that different values of (M_0, U) can correspond to the same (f_0, U) and, consequently, to the *same* Lynden-Bell equilibrium (see Sec. II D). Therefore, the use of these variables leads to some redundancies. Nevertheless, their advantage is that they are more directly related to physically accessible parameters. In any case, it is of interest to compare the two phase diagrams in (f_0, U) and (M_0, U) planes to see their similarities and differences.

For the rectangular water-bag initial condition, using Eqs. (17) and (18), we can express f_0 as a function of M_0 and U by

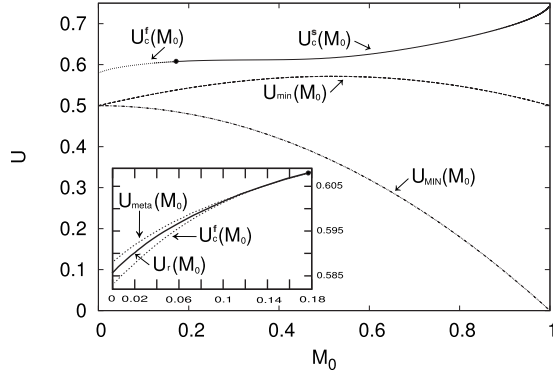


FIG. 3. Phase diagram in the control parameter plane (M_0, U) for a rectangular water-bag initial profile. $U_{MIN}(M_0)$ is the absolute minimum energy, and the homogeneous phase only exists above the line $U_{min}(M_0)$. The stability curve $U_c(M_0)$ is parameterized by λ . For $\lambda \rightarrow 0$ (completely degenerate limit), we get $M_0=0$ and $U_c=7/12$. For $\lambda \rightarrow +\infty$ (nondegenerate limit), we get $M_0=1$ and $U_c=3/4$. Above this curve, the homogeneous phase is stable and below this curve it is unstable. The full dot is the tricritical point. In the inset is showed the region of the first-order phase transition, indicated by the line $U_r(M_0)$, connected to the second-order phase transition line $U_c^s(M_0)$ by the tricritical point. The dotted lines are the borders of the metastability region.

$$f_0^2 = \frac{1}{48[(2U-1)(\Delta\theta)^2 + \sin^2 \Delta\theta]}, \quad (20)$$

where $\Delta\theta$ is related to M_0 by Eq. (19). Inserting this expression in Eqs. (12) and (13), we obtain after some algebra the caloric curve $\beta(U)$ for fixed M_0 parameterized by λ

$$U - \frac{1}{2} = \frac{\sin^2 \Delta\theta}{\frac{\pi^2 I_{-1/2}(\lambda)^3}{6 I_{1/2}(\lambda)} - 2(\Delta\theta)^2}, \quad (21)$$

$$\beta = \frac{1}{\sin^2 \Delta\theta} \left(\frac{\pi^2}{6} I_{-1/2}(\lambda)^2 - 2(\Delta\theta)^2 \frac{I_{1/2}(\lambda)}{I_{-1/2}(\lambda)} \right). \quad (22)$$

The homogeneous Lynden-Bell distribution with fixed M_0 exists if and only if

$$U \geq U_{min}(M_0) \equiv \frac{1}{2} \left(\frac{\sin^2 \Delta\theta}{\pi^2 - (\Delta\theta)^2} + 1 \right). \quad (23)$$

On the other hand, regrouping all the preceding results, the critical curve $U_c(M_0)$ separating stable and unstable homogeneous Lynden-Bell distributions is given by the parametric Eqs. (12), (15), (20), and (19) where λ goes from 0 to $+\infty$.

The phase diagram of the Lynden-Bell distribution in the (M_0, U) plane is represented in Fig. 3. We have first plotted the minimum accessible energy of the homogeneous phase $U_{min}(M_0)$ defined by Eq. (23). We have also plotted the stability curve $U_c(M_0)$ of the homogeneous phase parameterized by λ . Above this curve the homogeneous ($M_{QSS}=0$) phase is stable (maximum entropy state) and below this curve it is unstable (saddle point of entropy). For $M_0=1$, we are in the nondegenerate limit $\lambda \rightarrow +\infty$ (because $f_0 \rightarrow +\infty$) and the critical energy is $U_c=3/4$ (Maxwell distribution). For $M_0=0$, we are in the completely degenerate limit $\lambda=0$ and

the critical energy is $U_c=7/12$ (spatially homogeneous water bag).

If we now take into account Lynden-Bell's inhomogeneous states, solving numerically Eqs. (9), we find that the phase diagram displays first- and second-order phase transitions. The second-order phase transition corresponds to the branch $U_c^s(M_0)$ and the first-order phase transition to the branch $U_r(M_0)$. These two lines merge together at the tricritical point, located at $((M_0)_*, U_*) \simeq (0.1757, 0.608)$ corresponding to $\Delta\theta_* = 2.656\dots$ Using Eq. (20), we readily check that this tricritical point $((M_0)_*, U_*)$ corresponds to the tricritical point $((f_0)_*, U_*)$ in the (f_0, U) plane. We have also plotted in the inset the lateral edges $U_r^f(M_0)$ and $U_{meta}(M_0)$ of the metastability region associated with the first-order phase transition.

Therefore, the phase diagrams in (f_0, U) and (M_0, U) planes are fully consistent (see Sec. II D for more details) and both display first- and second-order phase transitions. The correctness of the above analysis is assessed in Ref. [25] where numerical simulations are performed for different values of the system size N . The transitions predicted in the realm of Lynden Bell's theory are indeed numerically observed, thus confirming the adequacy of the proposed interpretative scenario. Note, however, that the physics is different whether we vary the energy at fixed f_0 or at fixed M_0 . In particular, there is a "re-entrant" phase when we vary the energy at fixed f_0 [22] but there is no re-entrant phase when we vary the energy at fixed M_0 [25].

D. Connection between the two phase diagrams

To make the connection between the phase diagram (f_0, U) of Sec. II B and the phase diagram (M_0, U) of Sec. II C, we can plot the iso- M_0 lines in the (f_0, U) phase diagram or the iso- f_0 lines in the (M_0, U) phase diagram.

Let us first consider the iso- M_0 lines in the (f_0, U) phase diagram. If we fix the initial magnetization M_0 , or equivalently if we fix the parameter $\Delta\theta$, the relation between the energy U and f_0 is

$$U_{\Delta\theta}(f_0) = \frac{1}{6(4\Delta\theta f_0)^2} - \frac{1}{2} \left(\frac{\sin \Delta\theta}{\Delta\theta} \right)^2 + \frac{1}{2}. \quad (24)$$

Therefore, the iso- M_0 lines are of the form

$$U_{\Delta\theta}(f_0) = \frac{A(\Delta\theta)}{f_0^2} - B(\Delta\theta), \quad (25)$$

with $A(\Delta\theta) = \frac{1}{6(4\Delta\theta)^2}$ and $B(\Delta\theta) = \frac{1}{2} \left(\frac{\sin \Delta\theta}{\Delta\theta} \right)^2 - \frac{1}{2}$, which are easily represented in the (f_0, U) phase diagram (see Fig. 4). Figure 4 is in good agreement with the structure of the phase diagram in the (M_0, U) plane. Indeed, along an iso- M_0 line, we find that for large energies $U > U_c(M_0)$ the homogeneous phase is stable and for low-energies $U < U_c(M_0)$ the homogeneous phase becomes unstable. In that case, there is no re-entrant phase. We also note that for $M_0 < (M_0)_*$, the phase transition goes from second order to first order. This corresponds to the case where the iso- M_0 line crosses the tricritical point.

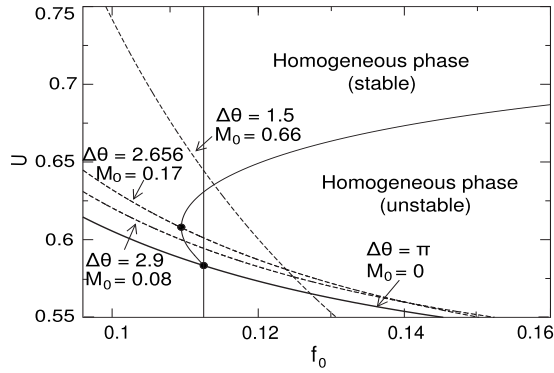


FIG. 4. Iso- M_0 lines in the (f_0, U) phase diagram. This graphical construction allows one to make the connection between the (f_0, U) phase diagram of Fig. 2 and the (M_0, U) phase diagram of Fig. 3. We can vary the energy at fixed initial magnetization by following a dashed line. The intersection between the dashed line and the curve $U_{\min}(f_0)$ determines the minimum-energy $U_{\min}(M_0)$ of the homogeneous phase. The intersection between the dashed line and the curve $U_c(f_0)$ determines the energy $U_c(M_0)$ below which the homogeneous phase becomes unstable.

Remark: we see on Fig. 4 that different iso- M_0 lines can cross each other. This means that different initial conditions (M'_0, U) and (M''_0, U) can correspond to the same (f_0, U) hence to the same Lynden-Bell distribution. In other words, in Lynden-Bell's theory the couples (M'_0, U) and (M''_0, U) are equivalent. There is therefore some redundancy in using the variables (M_0, U) instead of the variables (f_0, U) . Note, however, that the Lynden-Bell prediction does not always work so that, in case of incomplete relaxation, the couples (M'_0, U) and (M''_0, U) may lead to different QSS. However, this happens for $f_0 \geq 0.11053\dots$, i.e., in a parameter range which is only marginally interesting for our analysis.

Let us now consider the iso- f_0 lines in the (M_0, U) phase diagram. If we fix the phase level f_0 , the relation between the energy U and M_0 , or equivalently $\Delta\theta$, is

$$U_{f_0}(\Delta\theta) = \frac{1}{6(4\Delta\theta f_0)^2} - \frac{1}{2} \left(\frac{\sin \Delta\theta}{\Delta\theta} \right)^2 + \frac{1}{2}. \quad (26)$$

Therefore, the iso- f_0 lines are of the form

$$U_{f_0}(\Delta\theta) = \frac{C(f_0)}{(\Delta\theta)^2} - \frac{1}{2} \left(\frac{\sin \Delta\theta}{\Delta\theta} \right)^2 + \frac{1}{2}, \quad (27)$$

with $C(f_0) = \frac{1}{6(4f_0)^2}$, which are easily represented in the (M_0, U) phase diagram (Fig. 5). Recall that $\Delta\theta$ is related to M_0 by Eq. (19). Figure 5 is in good agreement with the structure of the phase diagram in the (f_0, U) plane. In particular, we can see that for a set of values of $f_0 \in [(f_0)_*, (f_0)_c]$, it intersects the curve $U_c(M_0)$ twice leading to re-entrant phases. We also note that the iso- f_0 lines cannot cross each other contrary to the iso- M_0 lines.

E. Determination of the absolute minimum energy in the (f_0, U) plane for a rectangular water-bag initial condition

We recall that homogeneous Lynden-Bell distributions exist only for $U > U_{\min}(f_0)$. However, there can exist inhomogeneous Lynden-Bell distributions for $U < U_{\min}(f_0)$. Let us determine the minimum accessible energy $U_{MIN}(f_0)$ when we start from a rectangular water-bag initial condition. For fixed f_0 the energy of the initial condition is a function of $\Delta\theta$ (or initial magnetization M_0) given by

$$U_{f_0}(\Delta\theta) = \frac{1}{6(4\Delta\theta f_0)^2} - \frac{1}{2} \left(\frac{\sin \Delta\theta}{\Delta\theta} \right)^2 + \frac{1}{2}. \quad (28)$$

We thus have to determine the minimum of this function for $0 \leq \Delta\theta \leq \pi$. First of all, the condition $U'_{f_0}(\Delta\theta) = 0$ is equivalent to

$$f_0 = \frac{1}{\sqrt{48 \sin(\Delta\theta) [\sin(\Delta\theta) - \Delta\theta \cos(\Delta\theta)]}}. \quad (29)$$

This function is represented in Fig. 6. For $f_0 < 0.11053\dots$ there is no solution and for $f_0 > 0.11053\dots$ there are two solutions $\Delta\theta_1$ and $\Delta\theta_2$ corresponding to one local minimum and one local maximum (see Fig. 7). For $f_0 = 0.11053\dots$, we have $\Delta\theta_1 = \Delta\theta_2 = 2.2467\dots$. Then, we find that the local minimum is the absolute minimum if $U_{f_0}(\Delta\theta_1) < U_{f_0}(\pi)$. This is the case if $f_0 > (f_0)_m = 0.12135\dots$ corresponding to an energy

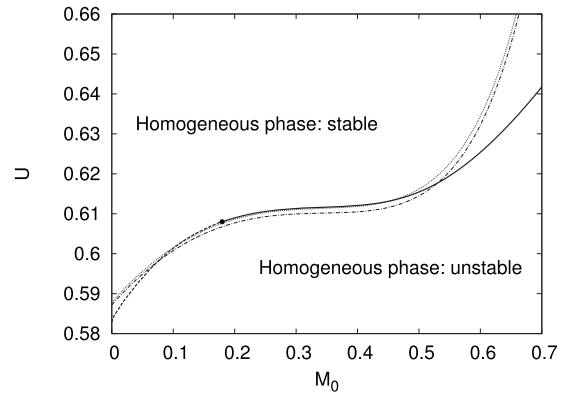


FIG. 5. Stability diagram in the (M_0, U) plane, with iso- f_0 lines. The thick lines are the two parts of the stability curve, the dotted line is the iso- f_0 line with $f_0 = 0.1096$ and the dash-dotted line is the iso- f_0 line with $f_0 = 0.1100$.

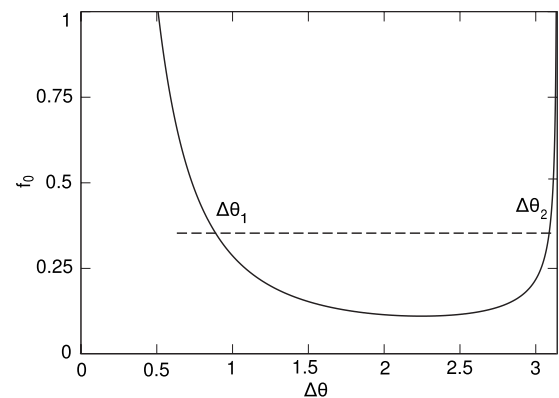


FIG. 6. Graphical construction determining the solutions of the equation $U'_{f_0}(\Delta\theta) = 0$.

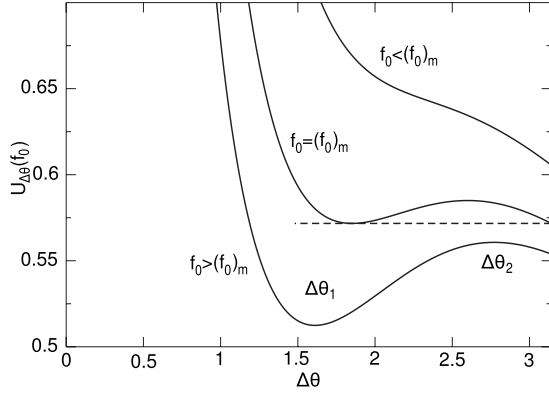


FIG. 7. Energy of the initial condition as a function of $\Delta\theta$ for different values of f_0 . From top to bottom: $f_0=0.10$, $f_0=(f_0)_m$, $f_0=0.12135$, and $f_0=0.14$.

$U_m=0.57167\dots$ (see Fig. 7). For $f_0 < (f_0)_m$, the absolute minimum corresponds to $\Delta\theta=\pi$.

In conclusion, for $f_0 < (f_0)_m$, we find that $U_{MIN}(f_0) = U_{f_0}(\pi)$ so that

$$U_{MIN}(f_0) = U_{\min}(f_0) = \frac{1}{96\pi^2 f_0^2} + \frac{1}{2}. \quad (30)$$

For $f_0 > (f_0)_m$, we find that $U_{MIN}(f_0) = U_{f_0}(\Delta\theta_1)$ where $\Delta\theta_1$ is the smallest root of Eq. (29). Combining these equations, we find that the absolute minimum-energy $U_{MIN}(f_0)$ is given in parametric form by

$$U_{MIN} = \frac{1}{2} \left(1 - \frac{\sin(2\Delta\theta_1)}{2\Delta\theta_1} \right), \quad (31)$$

$$f_0 = \frac{1}{\sqrt{48 \sin(\Delta\theta_1) [\sin(\Delta\theta_1) - \Delta\theta_1 \cos(\Delta\theta_1)]}}, \quad (32)$$

with $0 \leq \Delta\theta_1 \leq 1.85063\dots$. For $f_0 \rightarrow +\infty$ (nondegenerate limit), we get $\Delta\theta_1 \rightarrow 0$ and $U_{MIN}(f_0) \rightarrow 0$. This is the energy corresponding to an initial condition $f(\theta, p, t=0) = \delta(p) \delta(\theta)$.

Remark: for $f_0 > 0.11053$, we confirm on Fig. 7 that there can exist several initial conditions with the same f_0 and U but a different initial magnetization M_0 . They lead to the same Lynden-Bell prediction.

III. NUMERICAL RESULTS

To assess the correctness of the above theoretical prediction about the existence of a phase re-entrance, we have performed direct numerical simulations of the HMF model (1) for finite N . For that, we have chosen f_0 in the interval $(f_0)_* < f_0 < (f_0)_c$ and ran simulations at different energies. Results for $f_0=0.1096$ are shown in Fig. 8, where both the theoretical and numerical values of magnetization at the QSS, M_{QSS} , are plotted as a function of the energy.

Simulations (dashed line) confirm the existence of a regime of phase re-entrance. However, the agreement with theory (continuous line) is mainly qualitative, as there is a systematic shift between the two curves, although the mag-

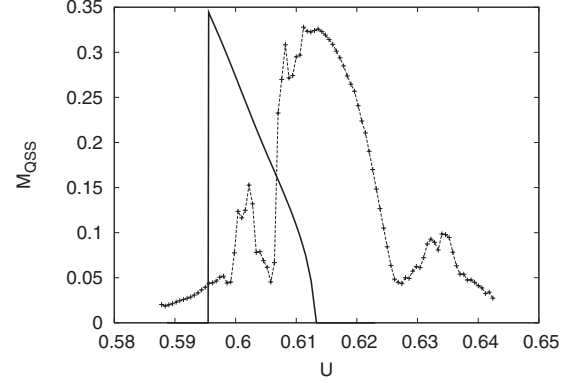


FIG. 8. Magnetization value at QSS, M_{QSS} , versus energy for $f_0=0.1096$. Comparison between theory (continuous line) and simulations (dashed line). Simulations, done with $N=10^6$, are performed using a symplectic integration algorithm, and averaging the magnetization over the time window $40 < t < 140$, and over 50 different realizations. For this f_0 , $U_{\min}=0.5878$, $U_r=0.5955$, $U_c^f=0.6026$, and $U_c^s=0.6131$.

netization value of the main bump is consistent with the one predicted from Lynden-Bell's approach. Moreover, simulations show the existence of two zones of magnetization revival at both sides of the central magnetized region. If we move at $f_0=0.1100$ (Fig. 9), we find that one of the two bumps has grown; this confirms that the structure of the phase diagram is more complex than predicted by the theory, as we find the existence of additional phase re-entrances. Simulations performed using different numbers of particles show that the magnetization values of the central magnetized region and of the two bumps do not depend on the system size. Instead, as expected, the curve offset goes to zero when the system size is increased (see Fig. 9).

A possible explanation for the discrepancies between theory and simulations can be found by considering that the energy range in which phase re-entrance is observed is quite narrow. In fact, the iso- f_0 lines, in the interval $(f_0)_* < f_0 < (f_0)_c$, are very close to the theoretical phase-transition curve (see Fig. 5). This means that any possible (i.e., even

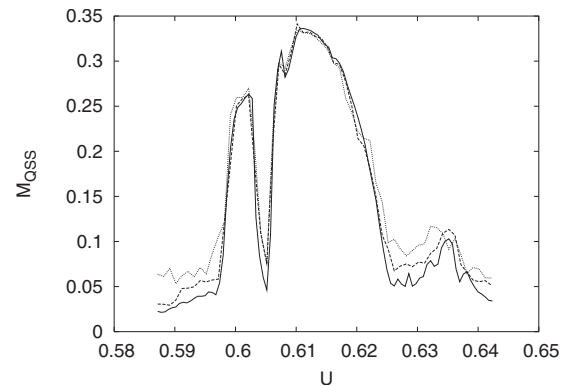


FIG. 9. Magnetization value at QSS, M_{QSS} , versus energy for $f_0=0.1100$. For this f_0 , $U_{\min}=0.5872$, $U_c^f=0.5980$, and $U_c^s=0.6177$. We plotted it for different sizes of the system: the continuous line corresponds to $N=10^6$, the dashed line to $N=5 \cdot 10^5$ and the dotted line to $N=10^5$.

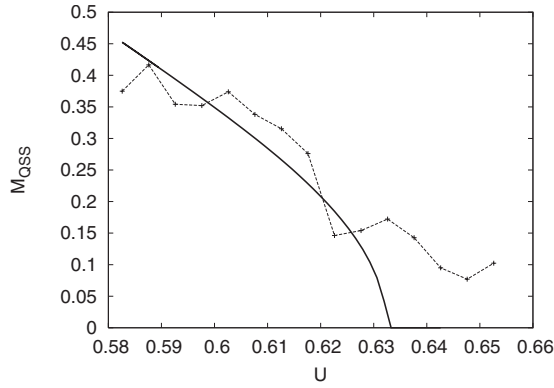


FIG. 10. Magnetization value, M_{QSS} , versus energy for $f_0 = 0.1130 > (f_0)_c$. Comparison between theory (continuous line) and simulations (dotted line). $U_{\min} = 0.5826$ and $U^s = 0.6325$.

small) disagreement between the theoretical and the numerical one may easily lead: (a) to a further numerical phase re-entrance, if the iso- f_0 line crosses the numerical phase-transitions curves without crossing the theoretical one; (b) to a larger numerical value of M_{QSS} , if the iso- f_0 separates from the numerical curve, while staying close to the theoretical one.

We also compared theory and simulations for higher f_0 ($> (f_0)_c$). As shown in Fig. 10, here theoretical and numerical results are close. This is in agreement with what is reported in Ref. [25]. In Fig. 11, we plotted our numerical results for a f_0 lower than $(f_0)_*$. For $f_0 = 0.1085$, close to the critical line $U_c(f_0)$, we observe a magnetized phase although Lynden-Bell’s approach predicts a nonmagnetized phase. For lower values of f_0 , homogeneous QSS are observed in agreement with the theoretical prediction (data not shown).

To provide a complete picture of the whole phase diagram, we carried out simulations on a grid in the (f_0, U) plane and plotted the numerically obtained values of M_{QSS} in color scale (see Fig. 12). At first order, we observe a fair agreement between theory and simulations. In particular, the predicted re-entrant phase phenomenon is clearly observed. This can be considered as a success of the Lynden-Bell theory. We also note that the region (III) of the phase dia-

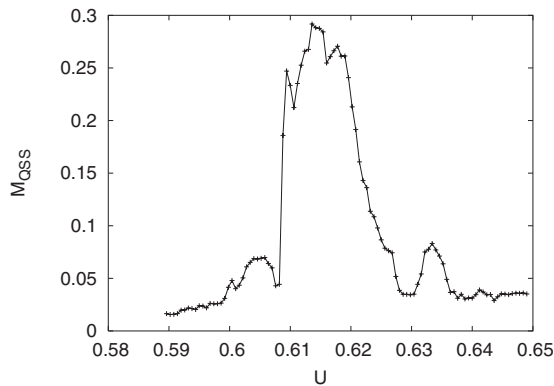


FIG. 11. Magnetization value, M_{QSS} , versus energy for $f_0 = 0.1085 < (f_0)_*$. For $f_0 < (f_0)_*$, the Lynden-Bell approach predicts that the QSS should be nonmagnetized so there is a disagreement with theory when f_0 is close to the tricritical point.

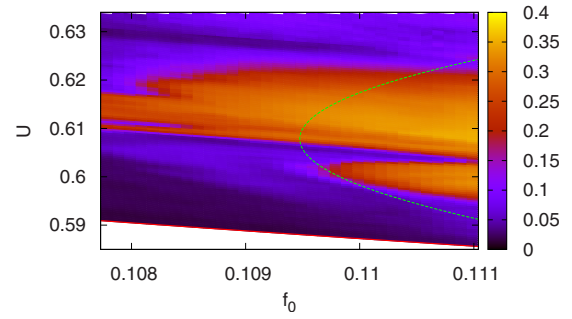


FIG. 12. (Color online) Stability diagram in the f_0 - U space with numerically calculated mean magnetizations. The dashed line is the stability curve. The theoretical re-entrant phase is clearly visible as well as the second (unexpected) re-entrant phase. In addition to this interesting new re-entrance phase, the other main discrepancy is the persisting magnetized phase for low f_0 .

gram appears to be nonmagnetized. It corresponds therefore to a local Lynden-Bell entropy maximum. This confirms our claim about the robustness of metastable states. Note, however, that starting from different initial conditions (with identical values of U and f_0), we could have found that the QSSs in this region are magnetized. Indeed, in the metastability region, the selection between local (metastable) or global (state) entropy maxima depends on a complicated notion of basin of attraction. Furthermore, we also find some unpredicted phenomena, as the additional phase re-entrance, for $U \approx 0.605$ (see also Fig. 9) and a persisting magnetized phase for low f_0 (see also Fig. 11).

We also studied the order of phase transitions, by plotting the probability histogram of M_{QSS} sampled with 300 different realizations. We show the results for two of the transitions occurring in Fig. 9. In Fig. 13, one can see that for the transition at $U \approx 0.5980$, distributions are characterized by a double peak, which is a clear signature of a first-order phase transition. For the one at $U \approx 0.6230$ (see Fig. 14), the distributions are instead characterized by a single peak, which validates the prediction of a second-order phase transition. The two transitions at the boundaries of the smaller phase

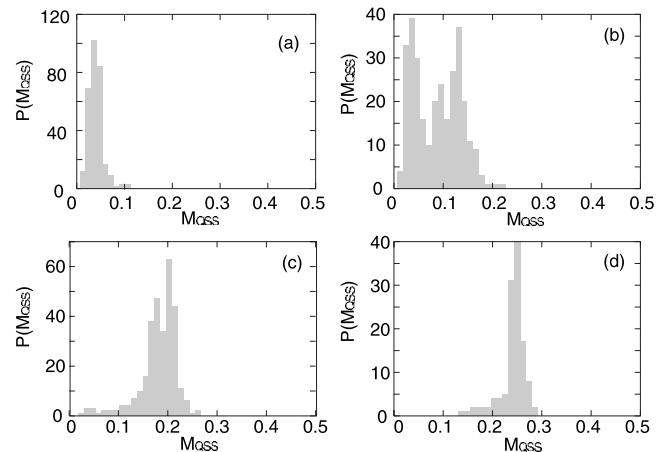


FIG. 13. Probability distributions of M_{QSS} for different U values at $f_0 = 0.1100$. Here in (a) $U = 0.5970$, in (b) $U = 0.5980$, (c) $U = 0.5990$, and in (d) $U = 0.6000$.

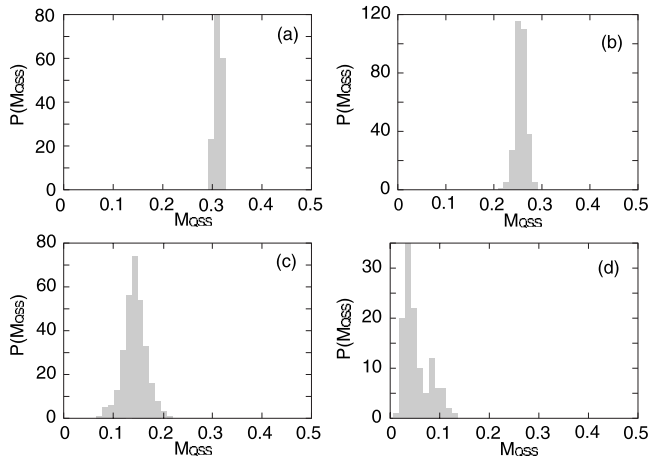


FIG. 14. Probability distributions of M_{QSS} for different U values at $f_0=0.1100$. Here in (a) $U=0.6150$, in (b) $U=0.6190$, (c) $U=0.6230$, and in (d) $U=0.6270$.

re-entrance, occurring around $U \sim 0.605$, not predicted by the theory, are found to be of first (at low energy) and second (at high energy) order (data not shown).

Finally, we compared the analytical and numerical caloric curves $\beta(U)$ for a given value of f_0 . In the simulations, the temperature has been calculated from the usual expression

$$\frac{1}{\beta_{kin}} = \langle p^2 \rangle = \int d\theta dp \bar{f}_{QSS}(\theta, p) p^2. \quad (33)$$

We note that the “kinetic” temperature defined by Eq. (33) does not coincide with the Lagrange multiplier β associated with the energy conservation in the Lynden-Bell distribution (8). This is due to the fermionic nature of this distribution. Therefore, in order to make the comparison between simulations and theory relevant, we have calculated the theoretical temperature from the mean-square momentum (33) averaged with the Lynden-Bell distribution given by Eq. (8). The results are reported in Fig. 15. In continuity with the results of Fig. 8, the range of energies where the inhomogeneous phase appears is shifted with respect to the theoretical prediction. As a further point, we also notice the presence of a region with negative specific heat, both in the numerical and ana-

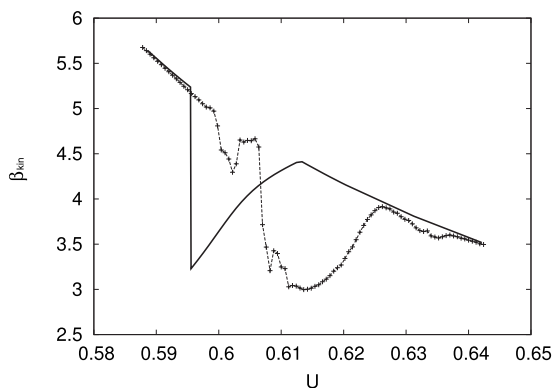


FIG. 15. Comparison between theoretical (continuous line) and numerical (dashed line) caloric curves, for $f_0=0.1096$.

lytical curves. To the best of our knowledge, this is the first time negative specific heat is observed out of equilibrium. Surprisingly, this phenomenon is here observed in correspondence of a second-order transition line.

IV. CONCLUSION

In this paper, we have confronted the predictions [22–26] of a theory based on Lynden-Bell’s statistical mechanics of violent relaxation [27] to the results of numerical experiments. The application of Lynden-Bell’s theory to the HMF model predicts a re-entrant phase in the (f_0, U) plane [22] and, indeed, we observe it. It occurs for a narrow range of parameters which would have been difficult to find without such a theoretical prediction. In this sense, this is a great success of Lynden-Bell’s approach. The theory also predicts the correct value of the magnetization in the inhomogeneous phase and the correct order of the phase transition. This is again remarkable because the phase diagram displays first and second-order phase transitions in a very narrow range of parameters (f_0, U) . All these predictions are confirmed by direct N -body experiments. We have also numerically observed that metastable states (local Lynden-Bell entropy maxima) can be very robust, so that they are stable in practice. This is a specificity of systems with long-range interactions [33,34].

However, we have also found some discrepancies with respect to Lynden-Bell’s theory. In particular, numerical simulations have demonstrated the existence of second re-entrant phases: a band of unmagnetized states in the theoretically magnetized region, as well as persisting magnetized states in the theoretically unmagnetized region. As a matter of fact, there is a systematic shift in the transition line with respect to theory. We must emphasize, however, the very small selected region of parameters in Figs. 8 and 12. This gives the impression of a big discrepancy although the discrepancy is in fact very small.

Therefore, from these numerical experiments, we can conclude that the Lynden-Bell statistical theory gives a fair first-order description of QSSs in the HMF model. However, for some initial conditions, there can be more or less severe discrepancies with respect to the prediction. This is a well-known fact in stellar dynamics [27] and vortex dynamics [18] to which this theory was initially applied (see a detailed discussion in Ref. [35]). Discrepancies with the Lynden-Bell theory have also been reported for the HMF model in Refs. [22,36]. These discrepancies are usually the result of an *incomplete relaxation* [27], i.e., a lack of efficient mixing in the system phase space. Indeed, the Lynden-Bell theory is based on a hypothesis of ergodicity and the prediction fails (by definition) if the evolution is not ergodic. A detailed understanding of incomplete violent relaxation is still lacking and appears to be very difficult [7].

Another cause of discrepancy may be related to the proximity of the numerically considered parameters (f_0, U) to the critical line and to the tricritical point. Indeed, it is well-known in equilibrium statistical mechanics that strong fluctuations are present close to a critical point, and that the

mean-field results cease to be valid in the vicinity of a critical point [37]. In the present case, we are studying out-of-equilibrium phase transitions and it is not clear if we can directly extend equilibrium results to that situation. Nevertheless, it is not unreasonable to expect that the theoretical results may be altered close to the critical line and this is

indeed what we observe numerically. Further away from the critical line (i.e., for larger or smaller values of f_0), we find a very good agreement with the Lynden-Bell prediction (see also [23]). These different observations concerning the success or the failure of the Lynden-Bell theory are consistent with the discussion given in [22].

-
- [1] C. Timm and C. J. Pye, Phys. Rev. B **77**, 214437 (2008).
 [2] C. Güven *et al.*, Phys. Rev. E **77**, 061110 (2008).
 [3] S. Han, S. Park, and B. Kim, Phys. Rev. E **79**, 066114 (2009).
 [4] M. Sellitto and J. Kurchan, Phys. Rev. Lett. **95**, 236001 (2005).
 [5] C. Ekiz, Phys. Lett. A **332**, 121 (2004).
 [6] L. Radzihovsky, EPL **36**, 595 (1996).
 [7] P. H. Chavanis *et al.*, Astrophys. J. **471**, 385 (1996).
 [8] T. Dauxois *et al.*, *Dynamics and Thermodynamics of Systems with Long Range Interactions*, Lecture Notes in Physics Vol. 602, (Springer, Berlin, 2002).
 [9] M. Hénon, Ann. Astrophys. **27**, 83 (1964).
 [10] F. Hohl and J. W. Campbell, Astron. J. **73**, 611 (1968).
 [11] A. Taruya and M. Sakagami, Mon. Not. R. Astron. Soc. **364**, 990 (2005).
 [12] J. Sommeria, C. Staquet, and R. Robert, J. Fluid Mech. **233**, 661 (1991).
 [13] R. Kawahara and H. Nakanishi, J. Phys. Soc. Jpn. **76**, 074001 (2007).
 [14] V. Latora *et al.*, Phys. Rev. Lett. **80**, 692 (1998).
 [15] Y. Y. Yamaguchi *et al.*, Physica A **337**, 36 (2004).
 [16] A. Campa, P. H. Chavanis, A. Giansanti, and G. Morelli, Phys. Rev. E **78**, 040102(R) (2008).
 [17] X. P. Huang and C. F. Driscoll, Phys. Rev. Lett. **72**, 2187 (1994).
 [18] H. Brands, P. H. Chavanis, R. Pasmanter, and J. Sommeria, Phys. Fluids **11**, 3465 (1999).
 [19] J. Barré, T. Dauxois, G. De Ninno, D. Fanelli, and S. Ruffo, Phys. Rev. E **69**, 045501(R) (2004).
 [20] C. Benedetti *et al.*, Physica A **364**, 197 (2006).
 [21] A. Campa *et al.*, *Dynamics and Thermodynamics of Systems with Long Range Interactions: Theory and Experiments*, AIP Conf. Proc. No. 970 (AIP, New York, 2008).
 [22] P. H. Chavanis, Eur. Phys. J. B **53**, 487 (2006).
 [23] A. Antoniazzi, D. Fanelli, J. Barre, P. H. Chavanis, T. Dauxois, and S. Ruffo, Phys. Rev. E **75**, 011112 (2007).
 [24] A. Antoniazzi, F. Califano, D. Fanelli, and S. Ruffo, Phys. Rev. Lett. **98**, 150602 (2007).
 [25] A. Antoniazzi, D. Fanelli, S. Ruffo, and Y. Y. Yamaguchi, Phys. Rev. Lett. **99**, 040601 (2007).
 [26] P. Chavanis, G. De Ninno, D. Fanelli, and S. Ruffo, in *Chaos, Complexity and Transport*, edited by C. Chandre, X. Leoncini, and G. Zaslavsky (World Scientific, Singapore, 2008), p. 3.
 [27] D. Lynden-Bell, Mon. Not. R. Astron. Soc. **136**, 101 (1967).
 [28] P. H. Chavanis, Ph.D. thesis, ENS Lyon, 1996.
 [29] M. Antoni and S. Ruffo, Phys. Rev. E **52**, 2361 (1995).
 [30] P. H. Chavanis, Physica A **359**, 177 (2006).
 [31] P. H. Chavanis, *Statistical Mechanics of Violent Relaxation in Stellar Systems*, edited by N. Antonic, C. J. van Duijn, W. Jager, and A. Mikelic, Proceedings of the Conference on Multiscale Problems in Science and Technology, (Springer, Berlin, 2002).
 [32] P. H. Chavanis *et al.*, Eur. Phys. J. B **46**, 61 (2005).
 [33] M. Antoni *et al.*, EPL **66**, 645 (2004).
 [34] P. H. Chavanis, Astron. Astrophys. **432**, 117 (2005).
 [35] P. H. Chavanis, Physica A **387**, 787 (2008).
 [36] R. Bachelard, C. Chandre, D. Fanelli, X. Leoncini, and S. Ruffo, Phys. Rev. Lett. **101**, 260603 (2008).
 [37] L. P. Kadanoff, *Statistical Physics Statics, Dynamics, and Renormalization* (World Scientific, Singapore, 2000).
 [38] These parameters are related to those introduced in Ref. [22] by $U = \epsilon/4 + 1/2$, $\beta = 2\eta$, $f_0 = \eta_0/N = \mu/(2\pi)$, $k = 2\pi/N$, $x = \Delta\theta$, $y = (2/\pi)\Delta p$, and the functions F in Ref. [24] are related to the Fermi integrals by $F_k(1/y) = 2^{(k+1)/2} y I_{(k-1)/2}(y)$.
 [39] Here, the term “unstable” means that the homogeneous Lynden-Bell distribution is not a maximum entropy state, i.e. (i) it is not the most mixed state, and (ii) it is dynamically unstable with respect to the Vlasov equation. Hence, it should not be reached as a result of violent relaxation. One possibility is that the system converges to the spatially inhomogeneous Lynden-Bell distribution (8) with $M_{QSS} \neq 0$ which is the maximum entropy state (most mixed) in that case. Another possibility, always to consider, is that the system does not converge towards the maximum entropy state, i.e., the relaxation is incomplete (see Ref. [22]).